

Fully First-Principles Surface Spectroscopy with Machine Learning

Yair Litman,* Jinggang Lan, Yuki Nagata, and David M. Wilkins*




Cite This: *J. Phys. Chem. Lett.* 2023, 14, 8175–8182



Read Online

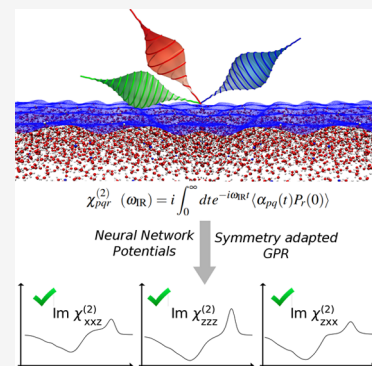
ACCESS |

 Metrics & More

 Article Recommendations

 Supporting Information

ABSTRACT: Our current understanding of the structure and dynamics of aqueous interfaces at the molecular level has grown substantially due to the continuous development of surface-specific spectroscopies, such as vibrational sum-frequency generation (VSFG). As in other vibrational spectroscopies, we must turn to atomistic simulations to extract all of the information encoded in the VSFG spectra. The high computational cost associated with existing methods means that they have limitations in representing systems with complex electronic structure or in achieving statistical convergence. In this work, we combine high-dimensional neural network interatomic potentials and symmetry-adapted Gaussian process regression to overcome these constraints. We show that it is possible to model VSFG signals with fully *ab initio* accuracy using machine learning and illustrate the versatility of our approach on the water/air interface. Our strategy allows us to identify the main sources of theoretical inaccuracy and establish a clear pathway toward the modeling of surface-sensitive spectroscopy of complex interfaces.



Soft matter interfaces, including aqueous interfaces, solid/liquid interfaces, and liquid/liquid interfaces, are ubiquitous in nature and play a crucial role in many important processes, such as (electro)catalytic/electrochemical applications,¹ atmospheric aerosol–gas exchanges,² and mineral dissolution.³ These processes are governed by the molecular level interaction between the molecules at the interface and the other (electrified) molecules/materials.

To probe the interfacial response, a technique must isolate the signal of the relatively few surface molecules at the surfaces from the enormous contribution due to the bulk.⁴ Vibrational sum frequency generation (VSFG) is a technique where IR and visible beams are spatially and temporally overlapped and the signal generated at the sum of the input beam frequencies is measured. VSFG is a second-order nonlinear optical process, and as in any other even-order nonlinear optical techniques, the centro-symmetric bulk contributions vanish due to the symmetry of the second-order susceptibility, $\chi^{(2)}$, making their signal surface-specific.⁵ The VSFG signal further possesses molecular specificity: a VSFG signal is enhanced when the IR frequency is resonant with an interfacial molecular vibration. When combining probes with different polarizations, VSFG can provide information on the orientation of interfacial molecules,^{6–8} the depth profile of the interfacial molecules,⁹ and molecular chirality.¹⁰ This makes VSFG a powerful method to characterize the identity, structure, and interaction of the molecules at interfaces.

Experimental VSFG data alone are normally insufficient to connect spectroscopic observables with molecular structure, and atomistic simulations are required to achieve a microscopic understanding. The theoretical calculation of VSFG spectra is more challenging than that of more traditional spectroscopies

such as linear IR and Raman, since relatively long simulation times (on the order of nanoseconds) are required to converge the statistics and guarantee that the signal in the bulk-like (centrosymmetric) regions vanishes.^{11,12}

The vibrational resonant component of the second-order susceptibility, $\chi_{pqr}^{(2)}$, in an electronically nonresonant condition, can be computed as¹¹

$$\chi_{pqr}^{(2)}(\omega_{IR}) = i \int_0^\infty dt e^{-i\omega_{IR}t} \langle \alpha_{pq}(t) P_r(0) \rangle \quad (1)$$

where α_{pq} is the pq component of the polarizability tensor, ω_{IR} is the frequency of the IR pulse, and P_r is the r component of the polarization vector. The evaluation of eq 1 requires an accurate representation of three objects, namely, (i) potential energy surface (PES), (ii) polarization surface (P -S), and (iii) polarizability surface (α -S).

Several approximations have been applied to calculate the VSFG spectrum of aqueous systems with varying degrees of success. The first group of studies use empirical polarizable models of the dipole moment and polarizability based on *ab initio* data.^{11–13} The drawback of such strategies is that accurate polarizable models are normally burdensome to construct and validate and cannot handle bond breaking or formation. The second group uses the projection of the transition dipole and polarizability moments into atomic

Received: July 18, 2023

Accepted: August 29, 2023

Published: September 6, 2023

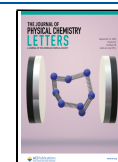


Table 1. Root Mean Squared Error (RMSE) for SA-GPR Models of Polarization per Atom (Debye) and Polarizability Per Atom (\AA^3)^a

Model Name	Reference	Configurations	Polarization (P)	Polarizability (α)
ML-POLY-A	POLY2VS	Bulk Water	7.6×10^{-4} (1.7%)	2.7×10^{-3} (13%)
ML-POLY-B	POLY2VS	Water Clusters	5.4×10^{-4} (0.5%)	2.2×10^{-3} (3%)
ML-PBE-A	DFT (PBE)	Bulk Water	1.0×10^{-3} (0.8%)	2.6×10^{-3} (13%)
ML-PBE0-A	DFT (PBE0)	Bulk Water	2.2×10^{-3} (0.8%)	–

^aNumbers in parentheses give the RMSE as a percentage of the intrinsic deviation in the training set.

velocities, leading to the surface-specific velocity–velocity correlation function formalism (ssVVCFF) approach.^{14,15} This approximation cannot predict the spectral differences observed with different combinations of laser polarization, since due to the approximations involved, it (incorrectly) predicts $\chi_{xxz}^{(2)} = \chi_{zzz}^{(2)}$ and $\chi_{zzz}^{(2)} = 0$. Furthermore, it is unable to capture important spectral features originating from vibrational coupling.^{16–18}

In this Letter, to overcome the problems inherent in “modeling the dipole moment and polarizability, the slow convergence of the time correlation function, and the accurate prediction of the VSG spectra at different polarization combinations, we propose the combination of several machine-learning (ML) methods. The PES is evaluated using either density functional theory (DFT) or Behler–Parrinello high-dimensional neural networks (HDNNPs),¹⁹ and P -S and α -S are evaluated by a symmetry-adapted Gaussian process regression (SA-GPR) scheme that enables the prediction of tensorial quantities of arbitrary order.^{20,21} The proposed scheme reduces the calculation cost of the fully first-principles modeling by more than 3 orders of magnitude, enabling the simulation of VSG spectra at various interfaces at any polarization combination.

The modeling of aqueous solution/air interfaces is normally performed by simulating the system under study in a slab geometry, in which the system extends infinitely along two dimensions and has finite size along the third dimension where it is sandwiched by regions of vacuum. This geometry gives rise to two interfaces that generate VSG signals with opposite signs that cancel each other and lead to a vanishing signal. Thus, it is not possible to obtain any meaningful spectra if one uses P and α of a total slab geometry in eq 1. As we discuss below, our ML approach offers an elegant and data-driven solution to this issue.

We start by describing the training of the P -S and α -S using SA-GPR. The reference data were obtained using DFT at the PBE and PBE0 level and POLY2VS, a polarizable water force field developed by Tanimura and co-workers.²² The PBE and PBE0 data sets are obtained from first-principles calculations and constitute the ultimate target of this work. The POLY2VS data set provides access to a molecular decomposition of the α and P quantities, allowing us to critically assess the performance of the ML models. Moreover, we considered two types of data sets, one made up exclusively of bulk structures and a second one made of water clusters from monomers up to hexamers (see a more detailed description of the data set and the training procedure in the Supporting Information).

In Table 1, we summarize the different models for the dielectric properties considered in this work. To enable comparisons between data sets, the error estimates are computed as the root-mean-square error (RMSE) percentage of the intrinsic deviation of the data set and expressed per water molecule. The SA-GPR models can accurately learn P and α with errors below a few percentages of intrinsic variation

in the training set. These values represent an error below 8.0×10^{-3} D/atom and 1×10^{-3} \AA^3 /atom for $|P|$ and $\text{Tr}[\alpha]$, respectively. In the Supporting Information, we report the correlation plots and learning curves of the ML models, together with a brief analysis of the training errors.

Global accuracy estimators, such as the RMSE and absolute error presented above, are useful indicators of the overall performance of the ML models. However, when the learned quantities are used for further calculations, as we do here for $\chi^{(2)}$, it is normally not possible to translate RMSE values directly into an objective accuracy measure of the final target. This is mainly because of the difficulty in performing a rigorous error propagation of the uncertainties in eq 1 but also due to the lack of a unique set of descriptors to quantify how “good” a predicted spectrum is. In this work, we take what we consider to be the strictest validation test and use VSG spectra to judge the accuracy of our models.

The calculation of $\chi^{(2)}$ for a slab geometry needs to be done with care since the contributions of opposite interfaces interfere destructively and lead to a vanishing response. Assuming that the slab thickness is large enough to accommodate a bulk region in the middle and that a molecular decomposition of P is available, it is standard practice to set to zero or flip the sign of the molecular dipoles below the center of mass of the slab to avoid this cancellation.^{14,15} However, molecular dipoles are not observables, and therefore, they are arbitrary in nature. In *ab initio* calculations the molecular decomposition can be achieved by using maximally localized Wannier functions,^{23,24} which incurs the difficulty of requiring direct *ab initio* simulations.²⁵ Here, we instead utilized an unbiased data-driven approach. Since we are using an atom-centered decomposition to represent the atomic environments, the SA-GPR predictions can be expressed as a sum of molecular contributions as

$$\mathbf{y}(\mathcal{X}) = \sum_{\gamma} \mathbf{y}(\mathcal{X}_{\gamma}) \quad (2)$$

where γ represents the set of indices that corresponds to a given molecule, and \mathcal{X} and \mathcal{X}_{γ} the atomic environment of the trial configuration and the atomic environment of the γ water molecule, respectively. In this way, SA-GPR can be applied to the calculation of VSG using eq 1 for slab geometries by applying the following modification to eq 2 for the P predictions

$$P(\mathcal{X}) = \sum_{\gamma} g(z_{\gamma})P(\mathcal{X}_{\gamma}) \quad (3)$$

where the surface plane is assumed to be parallel to the xy plane, z_{γ} is the z -coordinate of the γ molecule, and

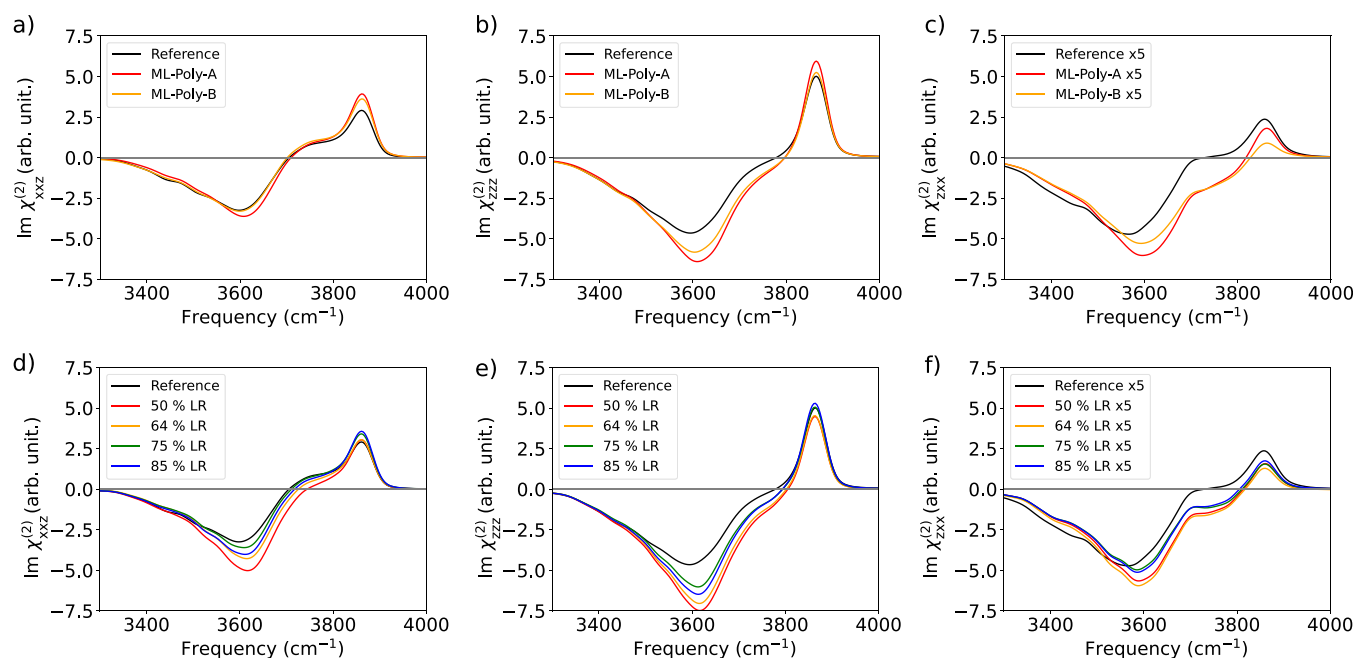


Figure 1. (a–c) Imaginary part of nonzero and independent $\chi^{(2)}$ components of the water/air interface using the POLY2VS model (reference) and ML-POLY-A and ML-POLY-B SA-GPR models. (d–f) Same as panels a–c but using ML-POLY-A augmented by different amounts of long-range (LR) contributions. $\chi_{zxx}^{(2)}$ spectra are multiplied by a factor of 5 to ease visualization.

$$g(z; z_1, z_2) = \begin{cases} \operatorname{sgn}(z - z_{\text{cm}}) & |z - z_{\text{cm}}| \geq z_1 \\ 0 & z_2 \geq |z - z_{\text{cm}}| \\ \operatorname{sgn}(z - z_{\text{cm}}) \cos\left(\frac{(z_1 - |z - z_{\text{cm}}|)\pi}{2(z_1 - z_2)}\right) & z_1 \geq |z - z_{\text{cm}}| \geq z_2 \end{cases} \quad (4)$$

where z_{cm} is the z -coordinate of the slab center of mass and z_1 and z_2 are two parameters that define the transition between the interfacial and bulk regions. The first condition in eq 4 flips the sign of the molecular contributions to the polarization that emerge from water molecules that are in the vicinity of the bottom interface, the second condition sets to zero the contributions to the polarization corresponding to water molecules that are in the vicinity of the slab center, and the third condition is a smooth transition between the previous two conditions. In this way, the signal of the opposite interfaces interfere constructively, leading to a nonvanishing VSGF signal.

Irrespective of the polarization, the $\operatorname{Im}\chi^{(2)}$ spectrum of the water/air interface presents a sharp positive peak centered at 3700 cm^{-1} and a broad band in the $3200\text{--}3500 \text{ cm}^{-1}$ region with a negative amplitude. The peak is due to the dangling (free) O–H group of the topmost interfacial water layer, and the band is associated with O–H groups of the interfacial water which form hydrogen bonds with other water molecules. The sign of the amplitudes in the $\operatorname{Im}\chi^{(2)}$ spectrum can be directly associated with the orientation of the water molecules. More specifically, positive (negative) amplitudes imply that the O–H group points toward the air (toward the bulk) phase. $\chi_{\text{pgr}}^{(2)}$ has only 3 independent elements: $\chi_{zzz}^{(2)}$, $\chi_{zxx}^{(2)}$, and $\chi_{xxz}^{(2)}$. $\chi_{zxx}^{(2)} = \chi_{zyy}^{(2)} = \chi_{zzx}^{(2)} = \chi_{yyz}^{(2)}$, and $\chi_{xxz}^{(2)} = \chi_{yyz}^{(2)}$ due to the xy plane being isotropic and the symmetry of the polarizability tensor. The rest of the elements are exactly zero except for large chiral environ-

ments.^{26,27} In the case of the water/air interface, the nonzero $\operatorname{Im}\chi^{(2)}$ tensor components differ essentially by the total intensity, the relative intensity of the free O–H and hydrogen-bonded O–H regions, and the presence or absence of a shoulder on the lower-frequency side of the free O–H peak.²⁸ Furthermore, the significantly small $\operatorname{Im}\chi_{yzy}^{(2)}$ spectrum compared with other polarization combinations is consistent with the experimental data.²⁹

We proceed now with a systematic evaluation of the ML predictions of the VSGF spectra. First, we consider a PES given by the POLY2VS force field and focus on the impact of the different models of α and P . Panels a–c in Figure 1 show $\chi_{xxz}^{(2)}$, $\chi_{zzz}^{(2)}$, and $\chi_{zxx}^{(2)}$, respectively. The ML-POLY-A and ML-POLY-B models are trained on POLY2VS reference data computed on bulk water and water cluster configurations, respectively (Table 1). As shown in Figure 1, both models have similar accuracy in their predictions of $\chi_{xxz}^{(2)}$ and $\chi_{zzz}^{(2)}$ and provide a semiquantitative agreement with the reference spectra. This is a rather surprising result since the ML-POLY-A model lacks information of interfacial water structures, whereas the ML-POLY-B model had only limited information on fully solvated water molecules. The prediction of $\chi_{zxx}^{(2)}$ is considerably worse than those of the other two tensor components, with ML-POLY-A performing only slightly better than ML-POLY-B for the free O–H peak. By performing cross-predictions using P/α from the ML model and α/P from the reference, we identified the α predictions as the source of the observed inaccuracy (see Figure S15). This result highlights the limitation of using RMSE values and correlation plots as error estimators, as all components of α show a comparable accuracy.

Electrostatic LR effects are known to play an important role at interfaces due to unbalanced interactions that can build up in the presence of a broken translation symmetry.³⁰ The implications of using short-range models on structural properties of the water/air interface, such as orientations of water molecules or average density are well documented.^{31,32}

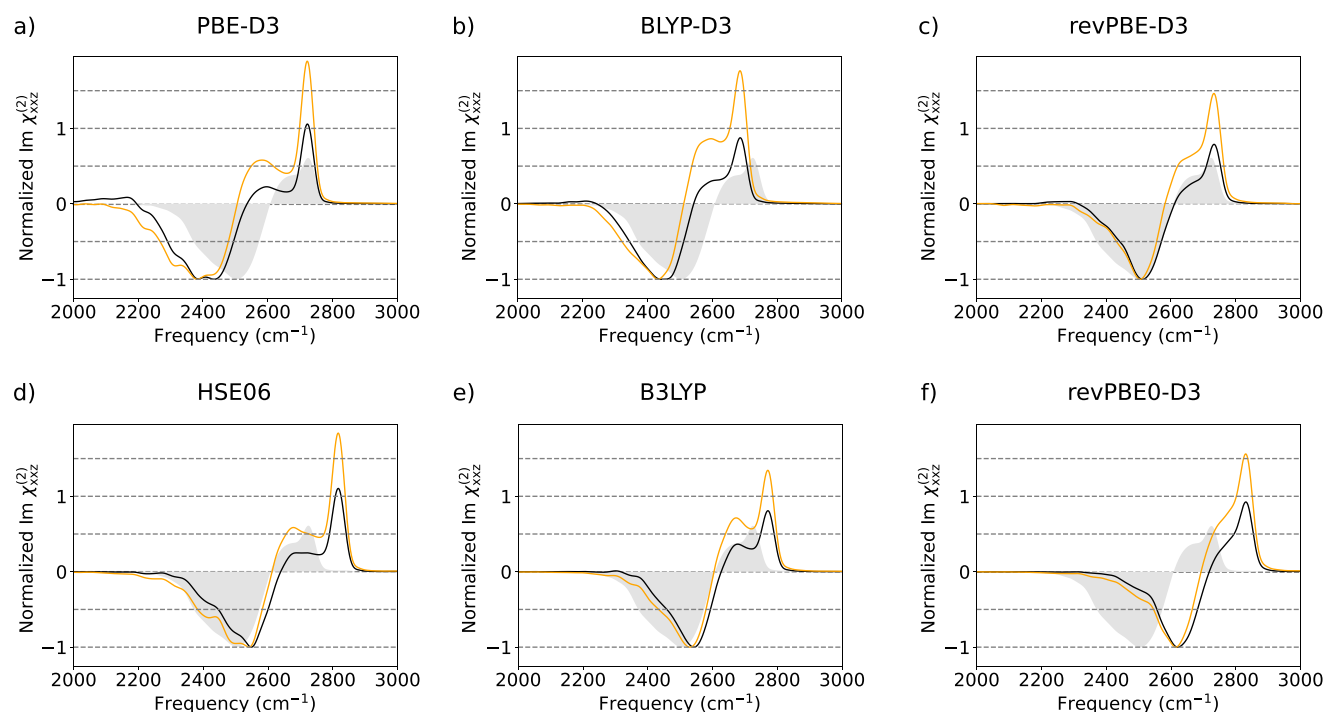


Figure 2. Simulated SFG spectra ($\chi_{xxz}^{(2)}$) of the water/air interface using trajectories obtained with *ab initio* PES and ML-PBE-A and ML-POLY-A are depicted by orange and black lines, respectively. Experimental spectra, corrected with Fresnel factors, assuming the Lorentz model for the interfacial dielectric constant, are depicted as gray shaded area.⁴⁴

ML models that include LR effects are also known to be more accurate.^{30,33} However, their possible impact on nonlinear spectroscopic responses, such as $\chi^{(2)}$, is less clear. To explore the magnitude of this effect, we trained a long-distance equivariant (LODE) model based on the local value of a atom-density potentials.³³ In Figure 1d–f, we show the predictions using a combination of short-range (SR) and LR contributions, since the combined model normally delivers a superior accuracy compared to the individual ones. In particular, we considered different amounts of LR contributions in the range of 50%–85%. The best combination across all the tensor components is obtained for a 25/75 SR/LR model, but the performance is very similar to that of SR models. These results unequivocally demonstrate that LR effects on the descriptions of P and α have a marginal impact on the $\chi^{(2)}$ spectra.

Having established the suitability of the training set and the methodology to describe P and α surfaces, we now consider the spectral changes induced by different *ab initio* PES. In Figure 2, we present the computed VSG spectra using SA-GPR response surfaces trained on PBE (ML-PBE-A) and POLY2VS (ML-POLY-A) data and six different *ab initio* potential energy surfaces, namely, PBE-D3, BLYP-D3, revPBE-D3, HSE06, B3LYP, and revPBE0-D3. The D₂O trajectories used for this analysis were available from a previous work.³⁴ Due to the limited length of the simulations, it was necessary to neglect intermolecular terms in eq 1 to obtain a reasonable converged spectrum (see more details in the Supporting Information). Thus, the width of the negative band is poorly described due to the absence of intermolecular couplings.¹⁴ In all cases except for PBE-D3, the spectra do not show a positive signal below 2200 cm⁻¹, in agreement with the latest measurements and simulations.^{35,36} For all the considered PESs, the ML-PBE-A model consistently overestimates (underestimates) the intensity of the free O–D peak (the

hydrogen bonded (HB) O–D band), while the ML-POLY-A model predicts relative intensities in better agreement with the experiments. The better performance of ML-POLY-A is a direct consequence of the fact that the reference POLY2VS dipole and polarizability surfaces were fitted to reproduce CCSD/aug-cc-pVQZ, rather than DFT, reference values. The calculations with GGA exchange correlation (XC) functionals (PBE-D3, BLYP, and revPBE-D3) are artificially red-shifted in comparison to the results obtained with hybrid ones (HSE06, B3LYP, and revPBE0-D3) in agreement with previous approximations based on the ssVVCf methodology³⁴ and results on bulk water.^{37,38} Inclusion of nuclear quantum effects (NQE) is known to induce a frequency red-shift when compared to the corresponding classical nuclei counterpart spectra.^{39,40} Thus, the frequency agreement between the revPBE-D3 PES and the experimental data is a fortuitous error compensation.³⁸

The intramolecular vibrational coupling of water molecules in which one O–D is a hydrogen-bond donor and the other one is free has a distinctive spectral feature associated with a shoulder on the free O–H peak. This shoulder has been assigned to the asymmetric stretching mode of interfacial water molecules,^{41,42} and contributions to this shoulder from water molecules forming two hydrogen bonds have been shown to be minor due to cancellation of inter- and intramolecular contributions.¹² PBE-D3, BLYP-D3, HSE06, and B3LYP spectra present a shoulder so separated from the free O–D peak that it can be regarded as a separate peak. In contrast, this spectral feature is correctly displayed by the revPBE0-D3 and revPBE-D3 spectra. Moreover, the differences in performance for revPBE0-D3 and revPBE-D3 are relatively small and mainly impact the intensity of the free O–D peak and an overall frequency shift. These results show that even hybrid func-

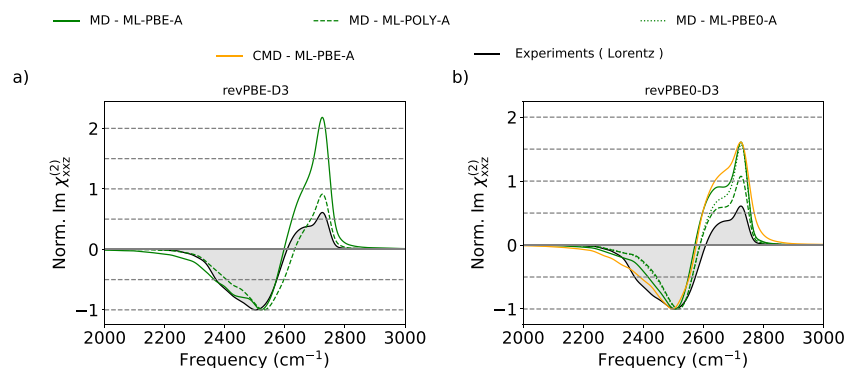


Figure 3. Normalized $\chi_{xxz}^{(2)}$ spectra of the D_2O /air interface at 300 K. Simulated spectra using revPBE-D3 (left) and revPBE0-D3 (right) XC functionals. Classical MD simulations using HDNNPs are presented by solid (ML-PBE-A), dashed (ML-POLY-A), and dotted (ML-PBE0-A) green lines. CMD simulations are depicted with solid orange lines. Experimental spectra are depicted as black solid lines with gray shading areas. Spectra were rigidly shifted to match experimental spectra. The values of the frequency shifts for revPBE0-D3 (revPBE-D3) are MD-HDNNP -138 cm^{-1} ($+4 \text{ cm}^{-1}$) and CMD-HDNNP -57 cm^{-1} . Experimental spectra are corrected by the appropriate Fresnel factors, assuming the Lorentz model (black dotted lines) for the interfacial dielectric constant.⁴⁴ To allow a visual comparative analysis, the spectra are normalized such that the HB O–D band has an intensity of unity.

tionals, such as HSE06 and B3LYP, considerably overestimate the H-bond strength, unlike in bulk water.⁴³

Finally, we show fully-ML predictions for the $\text{Im } \chi_{xxz}^{(2)}$ spectra for D_2O /air at 300 K in Figure 3 ($\text{Re } \chi_{xxz}^{(2)}$ is reported in the Supporting Information). We focus on HDNNP trained on revPBE0-D3⁴⁵ and revPBE-D3⁴⁶ XC functionals since this level of theory is known to describe the structure and dynamics of liquid water accurately.³⁸ The overall agreement between the spectra for each XC functional is remarkable when considering the computational costs associated with each type of calculation. The revPBE0-D3 HDNNP result shows a free O–D peak with a more pronounced shoulder and a blue-shift of 33 cm^{-1} with respect to the DFT prediction presented previously in Figure 2. Conversely, the revPBE-D3 HDNNP spectra show a less pronounced free O–D peak shoulder and a red-shift of -14 cm^{-1} . Both HDNNPs were trained without an explicit treatment of LR interactions, which are known, as mentioned previously, to be responsible for the net orientation of the water molecules in the bulk region. We believe that these artifacts are responsible for the (small) discrepancies with the fully *ab initio* spectra. In particular, the spurious additional orientation of water molecules, which happens in opposite directions for revPBE-D3 and revPBE0-D3 HDNNPs, as shown in Figure S17, might be responsible for increasing and decreasing the splitting between free and HB O–D vibrations of water molecules at the topmost layer. However, for all tested cases, irrespective of the PES, the theoretical predictions overestimate the intensity ratio between the free O–D and the hydrogen-bonded band. This underestimation has been reported by Paesani and co-workers when induction effects arising from interactions between individual molecules are neglected.⁴⁷ Since SA-GPR can capture local induction effects, the large discrepancy is attributed to the quality of the underlying reference data. Once more, the ML-POLY-A model outperforms ML-PBE-A. For the revPBE0-D3 case, we also tested the ML-PBE0-A model, in which the polarization was fitted to PBE0 reference data but the polarizability was kept at the PBE level. While it represents an improvement with respect to the ML-PBE-A model, particularly in the description of free O–D shoulder, it still underperforms compared to the ML-POLY-A results.

So far, we have analyzed simulations where the nuclei were assumed to behave classically, and the spectra have been rigidly red-shifted to account for the ignored NQEs. In the right panel of Figure 3, we show the results obtained with centroid molecular dynamics (CMD), which is a well-established method to simulate the vibrational spectra of condensed phase systems at room temperature including an approximate description of NQEs.^{48,49} CMD is based on the path integral formulation of quantum mechanics,⁵⁰ and in this method, the nuclei are evolved according to classical equations of motion on the so-called centroid potential of mean force. NQEs induce a broadening of the free O–D peak and HB-band and a red-shift of 81 cm^{-1} with respect to the corresponding classical nuclei simulations. However, the CMD spectrum is still blue-shifted by 57 cm^{-1} with respect to the experimental result. We also obtained the VSFG spectra using the thermostated ring polymer molecular dynamics (TRPMD)⁵¹ method which is known to deliver more accurate frequencies than CMD at 300 K since it does not suffer from the curvature problem^{49,52–54} (see Figure S19). By comparing the CMD and TRPMD results, we deduce that the curvature problem is responsible for an additional 10 cm^{-1} red-shift. We also compared with the latest refinement of the TRPMD method that employs thermostats based on the generalized Langevin equation that has been specifically designed to mitigate some of the artifacts associated with the original TRPMD formulation,⁵⁵ arriving to the same conclusion (see Figure S19). Thus, by accounting for the 33 cm^{-1} blue-shift induced by the lack of LR effects in the HDNNP discussed previously, we conclude that the error introduced by DFT in the revPBE0-D3 XC functional approximation is within the theoretical limit of quantum-statistical classical-dynamics methods which overestimate high-frequency modes by about 50 cm^{-1} .^{53,54}

The combination of two different types of ML algorithms, namely, HDNNPs and SA-GPR, has allowed us to describe the water/air interface and all the components (polarizations) of second-order response from first principles at an affordable computational cost. The ML models were trained in a general fashion, without employing specific information on the nature of the system, such as physical constraints designed for water, mapping models for water,⁵⁶ or the use of a Δ -ML procedure

based on an available surrogate model.⁵⁷ While at the moment force fields tailored to describe water outperform the presented results,^{12,28,44} we stress that the procedure and strategy presented are directly applicable to any reference data set, to larger systems, and most importantly, to more complex and reactive interfaces.

Several other ML approaches with varying architectures have been reported in the last five years to predict molecular dipole moments^{58–61} and linear vibrational spectroscopy.^{62–64} However, attempts to simulate VSFG spectroscopy have been lagging behind, most likely due to the destructive interference of the signal, which made those approaches inappropriate for this target. While the strategy presented here could be easily applied to other kernel regression models that use local representations, it remains to be seen if similar ideas could be implemented on neural network architectures.

We evaluated the impact of the different components that are involved in the calculation of the VSFG spectra. By comparing the performance of different XC functionals, we found that the PES is best described by the revPBE-D3 and revPBE0-D3 XC functionals. These results add to the existing evidence confirming that XC functionals constrained by exact functional conditions with suitable dispersion corrections, such as revPBE-D3 and revPBE0-D3, deliver excellent performance in the description of water.³⁸ Since the discrepancies between the theoretical and the experimental spectra are larger than the training error of the SA-GPR models, we attribute the largest source of error to the reference data used to describe the P and α surfaces. A further study using electronic structure methods beyond DFT to obtain more accurate P and α surfaces is urgently needed. We note that the modeling of the VSFG spectra described by eq 1 is derived in the electric dipole approximation.⁵ We believe that applying the current methodology to a more accurate reference data set would finally resolve existing controversies related to, for example, the relevance of quadrupole contributions in the water bending mode.^{65,66}

We showed that the off-diagonal components of the α tensor for water are more difficult to learn due to their smaller magnitude when compared to the diagonal ones, which leads to a poorer description of certain $\chi^{(2)}$ matrix elements. Since spherical components mix together diagonal and off-diagonal elements, it is not possible to train the off-diagonal elements exclusively with current SA-GPR implementations. Future efforts will be directed in this direction, in the development of machine learning models to predict Wannier centers,⁶⁷ atomic polar tensors,⁶⁸ and in the inclusion of explicit LR in the description of the PES.

Two different methods were considered to describe the time evolution of the nuclei: MD and CMD. CMD is appropriate to describe the D₂O/air interface and predicts a peak position that is in good agreement with experiments. However, the curvilinear motion of dangling O–D in D₂O shows an extremely broad feature,^{47,69} which calls for the use of other approaches which do not suffer from the curvature problem of CMD nor the broadening problem of TRPMD. The recent method proposed by Musil et al. seems a promising approach to tackle this issue.⁷⁰ We note, however, that none of these can describe accurately the Fermi resonance contributions.^{44,53,71,72}

In summary, the work presented here sets a new standard for atomistic simulation of nonlinear spectroscopies of condensed phases. While we have focused on the second-order response

which is related to VSFG spectroscopy, the approach presented here paves the way to *ab initio* simulations of 2D-VSFG, 2D-IR, 2D THz-Raman, and 2D THz-IR-Vis spectroscopies.^{73–75} We expect that applications of the presented strategy would bring important atomistic insights into the properties of aqueous interfaces at metallic and biological surfaces⁷⁶ in solution and under confinement.⁷⁷

■ ASSOCIATED CONTENT

Supporting Information

The Supporting Information is available free of charge at <https://pubs.acs.org/doi/10.1021/acs.jpcllett.3c01989>.

Detailed description of the VSFG calculations, learning curves, error analysis, and further validation tests (PDF)

Transparent Peer Review report available (PDF)

■ AUTHOR INFORMATION

Corresponding Authors

Yair Litman – Yusuf Hamied Department of Chemistry, University of Cambridge, Cambridge CB2 1EW, U.K.; Max Planck Institute for Polymer Research, 55128 Mainz, Germany; orcid.org/0000-0002-6890-4052; Email: yl899@cam.ac.uk

David M. Wilkins – Centre for Quantum Materials and Technologies School of Mathematics and Physics, Queen's University Belfast, Belfast BT7 1NN Northern Ireland, United Kingdom; orcid.org/0000-0003-3739-5512; Email: d.wilkins@qub.ac.uk

Authors

Jinggang Lan – Department of Chemistry, New York University, New York, New York 10003, United States; Simons Center for Computational Physical Chemistry at New York University, New York, New York 10003, United States; orcid.org/0000-0001-6353-2539

Yuki Nagata – Max Planck Institute for Polymer Research, 55128 Mainz, Germany; orcid.org/0000-0001-9727-6641

Complete contact information is available at:

<https://pubs.acs.org/doi/10.1021/acs.jpcllett.3c01989>

Notes

The authors declare no competing financial interest.

■ ACKNOWLEDGMENTS

Y.L. has been partly funded by the Deutsche Forschungsgemeinschaft (DFG, German Research Foundation) project number 467724959. D.M.W. thanks Queen's University Belfast for startup funding. J.L. thanks Simons Foundation Postdoctoral Fellowship. We thank Dr. Venkat Kapil for the useful discussion. We acknowledge the computing resources from the Swiss National Supercomputing Centre (CSCS) under project ID S1112 and S1113. Y.L. and Y.N. thank Mischa Bonn and Kuo-Yang Chiang for stimulating discussion and sharing the experimental data, and gratefully acknowledge the support from the MaxWater initiative from the Max Planck Society.

■ REFERENCES

- (1) Magnussen, O. M.; Groß, A. Toward an atomic-scale understanding of electrochemical interface structure and dynamics. *J. Am. Chem. Soc.* **2019**, *141*, 4777–4790.

- (2) Jubb, A. M.; Hua, W.; Allen, H. C. Environmental chemistry at vapor/water interfaces: insights from vibrational sum frequency generation spectroscopy. *Annu. Rev. Phys. Chem.* **2012**, *63*, 107–130.
- (3) Schott, J.; Pokrovsky, O. S.; Oelkers, E. H. The link between mineral dissolution/precipitation kinetics and solution chemistry. *Rev. Mineral. Geochem.* **2009**, *70*, 207–258.
- (4) Kraack, J. P.; Hamm, P. Surface-sensitive and surface-specific ultrafast two-dimensional vibrational spectroscopy. *Chem. Rev.* **2017**, *117*, 10623–10664.
- (5) Morita, A. *Theory of sum frequency generation spectroscopy*; Springer Nature Singapore: Singapore, 2018; pp 151–200.
- (6) Hore, D. K.; Beaman, D. K.; Parks, D. H.; Richmond, G. L. Whole-molecule approach for determining orientation at isotropic surfaces by nonlinear vibrational spectroscopy. *J. Phys. Chem. B* **2005**, *109*, 16846–16851.
- (7) Gan, W.; Wu, D.; Zhang, Z.; Feng, R.-R.; Wang, H.-F. Polarization and experimental configuration analyses of sum frequency generation vibrational spectra, structure, and orientational motion of the air/water interface. *J. Chem. Phys.* **2006**, *124*, 114705.
- (8) Zhuang, X.; Miranda, P. B.; Kim, D.; Shen, Y. R. Mapping molecular orientation and conformation at interfaces by surface nonlinear optics. *Phys. Rev. B* **1999**, *59*, 12632–12640.
- (9) Yu, C.-C.; Seki, T.; Wang, Y.; Bonn, M.; Nagata, Y. Polarization-dependent sum-frequency generation spectroscopy for ångstrom-scale depth profiling of molecules at interfaces. *Phys. Rev. Lett.* **2022**, *128*, 226001.
- (10) Konstantinovskiy, D.; Perets, E. A.; Santiago, T.; Velarde, L.; Hammes-Schiffer, S.; Yan, E. C. Y. Detecting the first hydration shell structure around biomolecules at interfaces. *ACS Cent. Sci.* **2022**, *8*, 1404–1414.
- (11) Morita, A.; Hynes, J. T. A theoretical analysis of the sum frequency generation spectrum of the water surface. ii. time-dependent approach. *J. Phys. Chem. B* **2002**, *106*, 673–685.
- (12) Moberg, D. R.; Straight, S. C.; Paesani, F. Temperature dependence of the air/water interface revealed by polarization sensitive sum-frequency generation spectroscopy. *J. Phys. Chem. B* **2018**, *122*, 4356–4365.
- (13) Nagata, Y.; Hsieh, C.-S.; Hasegawa, T.; Voll, J.; Backus, E. H. G.; Bonn, M. Water bending mode at the water–vapor interface probed by sum-frequency generation spectroscopy: a combined molecular dynamics simulation and experimental study. *J. Phys. Chem. Lett.* **2013**, *4*, 1872–1877.
- (14) Ohto, T.; Usui, K.; Hasegawa, T.; Bonn, M.; Nagata, Y. Toward ab initio molecular dynamics modeling for sum-frequency generation spectra; an efficient algorithm based on surface-specific velocity-velocity correlation function. *J. Chem. Phys.* **2015**, *143*, 124702.
- (15) Khatib, R.; Sulpizi, M. Sum frequency generation spectra from velocity–velocity correlation functions. *J. Phys. Chem. Lett.* **2017**, *8*, 1310–1314.
- (16) Tian, C.-S.; Shen, Y. R. Isotopic dilution study of the water/vapor interface by phase-sensitive sum-frequency vibrational spectroscopy. *J. Am. Chem. Soc.* **2009**, *131*, 2790–2791.
- (17) Nihonyanagi, S.; Ishiyama, T.; Lee, T.-k.; Yamaguchi, S.; Bonn, M.; Morita, A.; Tahara, T. Unified molecular view of the air/water interface based on experimental and theoretical $\chi(2)$ spectra of an isotopically diluted water surface. *J. Am. Chem. Soc.* **2011**, *133*, 16875–16880.
- (18) Yamaguchi, S.; Takayama, T.; Goto, Y.; Otsu, T.; Yagasaki, T. Experimental and theoretical heterodyne-Detected sum frequency generation spectroscopy of isotopically pure and diluted water surfaces. *J. Phys. Chem. Lett.* **2022**, *13*, 9649–9653.
- (19) Behler, J.; Parrinello, M. Generalized neural-network representation of high-dimensional potential-energy surfaces. *Phys. Rev. Lett.* **2007**, *98*, 146401.
- (20) Grisafi, A.; Wilkins, D. M.; Csányi, G.; Ceriotti, M. Symmetry-adapted machine learning for tensorial properties of atomistic systems. *Phys. Rev. Lett.* **2018**, *120*, 036002.
- (21) Deringer, V. L.; Bartók, A. P.; Bernstein, N.; Wilkins, D. M.; Ceriotti, M.; Csányi, G. Gaussian process regression for materials and molecules. *Chem. Rev.* **2021**, *121*, 10073.
- (22) Hasegawa, T.; Tanimura, Y. A polarizable water model for intramolecular and intermolecular vibrational spectroscopies. *J. Phys. Chem. B* **2011**, *115*, 5545–5553.
- (23) Wan, Q.; Galli, G. First-principles framework to compute sum-frequency generation vibrational spectra of semiconductors and insulators. *Phys. Rev. Lett.* **2015**, *115*, 246404.
- (24) Ojha, D.; Kühne, T. D. On-the-fly calculation of the vibrational sum-frequency generation spectrum at the air-water interface. *Molecules* **2020**, *25*, 3939.
- (25) Marx, D.; Hutter, J. *Ab initio molecular dynamics: basic theory and advanced methods*; Cambridge University Press: Cambridge, 2009.
- (26) Wang, J.; Chen, X.; Clarke, M. L.; Chen, Z. Detection of chiral sum frequency generation vibrational spectra of proteins and peptides at interfaces in situ. *Proc. Natl. Acad. Sci. U. S. A.* **2005**, *102*, 4978–4983.
- (27) Perets, E. A.; Olesen, K. B.; Yan, E. C. Y. Chiral sum frequency generation spectroscopy detects double-helix dna at interfaces. *Langmuir* **2022**, *38*, 5765–5778.
- (28) Chiang, K.-Y.; Seki, T.; Yu, C.-C.; Ohto, T.; Hunger, J.; Bonn, M.; Nagata, Y. The dielectric function profile across the water interface through surface-specific vibrational spectroscopy and simulations. *Proc. Natl. Acad. Sci. U. S. A.* **2022**, *119*, e2204156119.
- (29) Suzuki, Y.; Nojima, Y.; Yamaguchi, S. Vibrational coupling at the topmost surface of water revealed by heterodyne-detected sum frequency generation spectroscopy. *J. Phys. Chem. Lett.* **2017**, *8*, 1396–1401.
- (30) Niblett, S. P.; Galib, M.; Limmer, D. T. Learning intermolecular forces at liquid–vapor interfaces. *J. Chem. Phys.* **2021**, *155*, 164101.
- (31) Yue, S.; Muniz, M. C.; Calegari Andrade, M. F.; Zhang, L.; Car, R.; Panagiotopoulos, A. Z. When do short-range atomistic machine-learning models fall short? *J. Chem. Phys.* **2021**, *154*, 034111.
- (32) Gao, A.; Remsing, R. C. Self-consistent determination of long-range electrostatics in neural network potentials. *Nat. Commun.* **2022**, *13*, 1572.
- (33) Grisafi, A.; Ceriotti, M. Incorporating long-range physics in atomic-scale machine learning. *J. Chem. Phys.* **2019**, *151*, 204105.
- (34) Ohto, T.; Dodia, M.; Xu, J.; Imoto, S.; Tang, F.; Zysk, F.; Kühne, T. D.; Shigeta, Y.; Bonn, M.; Wu, X.; et al. Accessing the accuracy of density functional theory through structure and dynamics of the water–air interface. *J. Phys. Chem. Lett.* **2019**, *10*, 4914–4919.
- (35) Nihonyanagi, S.; Kusaka, R.; Inoue, K.-i.; Adhikari, A.; Yamaguchi, S.; Tahara, T. Accurate determination of complex $\chi(2)$ spectrum of the air/water interface. *J. Chem. Phys.* **2015**, *143*, 124707.
- (36) Tang, F.; Ohto, T.; Sun, S.; Rouxel, J. R.; Imoto, S.; Backus, E. H. G.; Mukamel, S.; Bonn, M.; Nagata, Y. Molecular structure and modeling of water–air and ice–air interfaces monitored by sum-frequency generation. *Chem. Rev.* **2020**, *120*, 3633–3667.
- (37) Gillan, M. J.; Alfè, D.; Michaelides, A. Perspective: How good is DFT for water? *J. Chem. Phys.* **2016**, *144*, 130901.
- (38) Marsalek, O.; Markland, T. E. Quantum dynamics and spectroscopy of ab initio liquid water: the interplay of nuclear and electronic quantum effects. *J. Phys. Chem. Lett.* **2017**, *8*, 1545–1551.
- (39) Markland, T. E.; Ceriotti, M. Nuclear quantum effects enter the mainstream. *Nat. Rev. Chem.* **2018**, *2*, 0109.
- (40) Benson, R. L.; Trenins, G.; Althorpe, S. C. Which quantum statistics—classical dynamics method is best for water? *Faraday Discuss.* **2020**, *221*, 350–366.
- (41) Schaefer, J.; Backus, E. H. G.; Nagata, Y.; Bonn, M. Both inter- and intramolecular coupling of o–h groups determine the vibrational response of the water/air interface. *J. Phys. Chem. Lett.* **2016**, *7*, 4591–4595.
- (42) Stiopkin, I. V.; Weeraman, C.; Pieniazek, P. A.; Shalhout, F. Y.; Skinner, J. L.; Benderskii, A. V. Hydrogen bonding at the water surface revealed by isotopic dilution spectroscopy. *Nature* **2011**, *474*, 192–195.

- (43) Guidon, M.; Schiffmann, F.; Hutter, J.; VandeVondele, J. Ab initio molecular dynamics using hybrid density functionals. *J. Chem. Phys.* **2008**, *128*, 214104.
- (44) Yu, X.; Chiang, K.-Y.; Yu, C.-C.; Bonn, M.; Nagata, Y. On the Fresnel factor correction of sum-frequency generation spectra of interfacial water. *J. Chem. Phys.* **2023**, *158*, 044701.
- (45) Schran, C.; Brezina, K.; Marsalek, O. Committee neural network potentials control generalization errors and enable active learning. *J. Chem. Phys.* **2020**, *153*, 104105.
- (46) Litman, Y.; Chiang, K.-Y.; Seki, T.; Nagata, Y.; Bonn, M. The surface of electrolyte solutions is stratified. *arXiv* **2022**, 2210.01527.
- (47) Medders, G. R.; Paesani, F. Dissecting the molecular structure of the air/water interface from quantum simulations of the sum-frequency generation spectrum. *J. Am. Chem. Soc.* **2016**, *138*, 3912–3919.
- (48) Habershon, S.; Fanourgakis, G. S.; Manolopoulos, D. E. Comparison of path integral molecular dynamics methods for the infrared absorption spectrum of liquid water. *J. Chem. Phys.* **2008**, *129*, 074501.
- (49) Rossi, M.; Liu, H.; Paesani, F.; Bowman, J.; Ceriotti, M. Communication: On the consistency of approximate quantum dynamics simulation methods for vibrational spectra in the condensed phase. *J. Chem. Phys.* **2014**, *141*, 181101.
- (50) Feynman, R. P.; Hibbs, A. R. *Quantum mechanics and path integrals*; McGraw-Hill: New York, 1965.
- (51) Rossi, M.; Ceriotti, M.; Manolopoulos, D. E. How to remove the spurious resonances from ring polymer molecular dynamics. *J. Chem. Phys.* **2014**, *140*, 234116.
- (52) Ivanov, S. D.; Witt, A.; Shiga, M.; Marx, D. Communications: on artificial frequency shifts in infrared spectra obtained from centroid molecular dynamics: quantum liquid water. *J. Chem. Phys.* **2010**, *132*, 031101.
- (53) Althorpe, S. C. Path-integral approximations to quantum dynamics. *Eur. Phys. J. B* **2021**, *94*, 155.
- (54) Trenins, G.; Willatt, M. J.; Althorpe, S. C. Path-integral dynamics of water using curvilinear centroids. *J. Chem. Phys.* **2019**, *151*, 054109.
- (55) Rossi, M.; Kapil, V.; Ceriotti, M. Fine tuning classical and quantum molecular dynamics using a generalized Langevin equation. *J. Chem. Phys.* **2018**, *148*, 102301.
- (56) Ni, Y.; Skinner, J. L. IR and SFG vibrational spectroscopy of the water bend in the bulk liquid and at the liquid-vapor interface, respectively. *J. Chem. Phys.* **2015**, *143*, 014502.
- (57) Qu, C.; Yu, Q.; Conte, R.; Houston, P. L.; Nandi, A.; Bomwan, J. M. A delta-machine learning approach for force fields, illustrated by a CCSD(T) 4-body correction to the MB-pol water potential. *Digital Discovery* **2022**, *1*, 658–664.
- (58) Veit, M.; Wilkins, D. M.; Yang, Y.; DiStasio, R. A., Jr.; Ceriotti, M. Predicting molecular dipole moments by combining atomic partial charges and atomic dipoles. *J. Chem. Phys.* **2020**, *153*, 024113.
- (59) Staacke, C. G.; Wengert, S.; Kunkel, C.; Csányi, G.; Reuter, K.; Margraf, J. T. Kernel charge equilibration: efficient and accurate prediction of molecular dipole moments with a machine-learning enhanced electron density model. *Mach. Learn.: Sci. Technol.* **2022**, *3*, 015032.
- (60) Christensen, A. S.; Faber, F. A.; von Lilienfeld, O. A. Operators in quantum machine learning: Response properties in chemical space. *J. Chem. Phys.* **2019**, *150*, 064105.
- (61) Gao, A.; Reimsing, R. C. Self-consistent determination of long-range electrostatics in neural network potentials. *Nat. Commun.* **2022**, *13*, 1572.
- (62) Gastegger, M.; Behler, J.; Marquetand, P. Machine learning molecular dynamics for the simulation of infrared spectra. *Chem. Sci.* **2017**, *8*, 6924–6935.
- (63) Han, B.; Isborn, C. M.; Shi, L. Incorporating polarization and charge transfer into a point-charge model for water using machine learning. *J. Phys. Chem. Lett.* **2023**, *14*, 3869–3877.
- (64) Sommers, G. M.; Calegari Andrade, M. F.; Zhang, L.; Wang, H.; Car, R. Raman spectrum and polarizability of liquid water from deep neural networks. *Phys. Chem. Chem. Phys.* **2020**, *22*, 10592–10602.
- (65) Kundu, A.; Tanaka, S.; Ishiyama, T.; Ahmed, M.; Inoue, K.-i.; Nihonyanagi, S.; Sawai, H.; Yamaguchi, S.; Morita, A.; Tahara, T. Bend vibration of surface water investigated by heterodyne-detected sum frequency generation and theoretical study: dominant role of quadrupole. *J. Phys. Chem. Lett.* **2016**, *7*, 2597–2601.
- (66) Seki, T.; Chiang, K.-Y.; Yu, C.-C.; Yu, X.; Okuno, M.; Hunger, J.; Nagata, Y.; Bonn, M. The bending mode of water: a powerful probe for hydrogen bond structure of aqueous systems. *J. Phys. Chem. Lett.* **2020**, *11*, 8459–8469.
- (67) Zhang, L.; Chen, M.; Wu, X.; Wang, H.; E, W.; Car, R. Deep neural network for the dielectric response of insulators. *Phys. Rev. B* **2020**, *102*, 041121.
- (68) Schienbein, P. Spectroscopy from machine learning by accurately representing the atomic polar tensor. *J. Chem. Theory Comput* **2023**, *19*, 705–712.
- (69) Kaliannan, N. K.; Aristizabal, A. H.; Wiebeler, H.; Zysk, F.; Ohto, T.; Nagata, Y.; Kühne, T. D. Impact of intermolecular vibrational coupling effects on the sum-frequency generation spectra of the water/air interface. *Mol. Phys.* **2020**, *118*, 1620358.
- (70) Musil, F.; Zaporozhets, I.; Noé, F.; Clementi, C.; Kapil, V. Quantum dynamics using path integral coarse-graining. *J. Chem. Phys.* **2022**, *157*, 181102.
- (71) Benson, R. L.; Althorpe, S. C. On the “Matsubara heating” of overtone intensities and Fermi splittings. *J. Chem. Phys.* **2021**, *155*, 104107.
- (72) Plé, T.; Huppert, S.; Finocchi, F.; Depondt, P.; Bonella, S. Anharmonic spectral features via trajectory-based quantum dynamics: A perturbative analysis of the interplay between dynamics and sampling. *J. Chem. Phys.* **2021**, *155*, 104108.
- (73) Perakis, F.; De Marco, L.; Shalit, A.; Tang, F.; Kann, Z. R.; Kühne, T. D.; Torre, R.; Bonn, M.; Nagata, Y. Vibrational spectroscopy and dynamics of water. *Chem. Rev.* **2016**, *116*, 7590–7607.
- (74) Savolainen, J.; Ahmed, S.; Hamm, P. Two-dimensional Raman-terahertz spectroscopy of water. *Proc. Natl. Acad. Sci. U. S. A.* **2013**, *110*, 20402–20407.
- (75) Grechko, M.; Hasegawa, T.; D’Angelo, F.; Ito, H.; Turchinovich, D.; Nagata, Y.; Bonn, M. Coupling between intra- and intermolecular motions in liquid water revealed by two-dimensional terahertz-infrared-visible spectroscopy. *Nat. Commun.* **2018**, *9*, 885.
- (76) Gonella, G.; Backus, E. H. G.; Nagata, Y.; Bonthuis, D. J.; Loche, P.; Schlaich, A.; Netz, R. R.; Kühnle, A.; McCrum, I. T.; Koper, M. T. M.; et al. Water at charged interfaces. *Nat. Rev. Chem.* **2021**, *5*, 466–485.
- (77) Kapil, V.; Schran, C.; Zen, A.; Chen, J.; Pickard, C. J.; Michaelides, A. The first-principles phase diagram of monolayer nanoconfined water. *Nature* **2022**, *609*, 512–516.